ϕ^4 Theory with Path-Integral MC on the Lattice

Projects for Computational Physics

Lukas Bayer & Jan Glowacz

March 7, 2021

Tutor: Nikolas Schlage

Contents

1 Introduction and Motivation

The so called ϕ^4 theory is the simplest interacting quantum field theory. Therefore it is commonly used as a toy model to study the basics of QFT like canonical quantization, Feynman diagrams, renormalization and the path integral formalism. The most important realization of ϕ^4 theory in the real world is the self-interaction of the Higgs field in the standard electroweak theory [1]. While ϕ^4 theory can be solved perturbatively, this project aims to demonstrate an alternative approach. Based on the path integral formalism, the theory is implemented on a discretized space-time lattice. Important quantum field theoretical quantities like the 2-point correlation function and the effective mass can then be extracted using a Markov chain Monte-Carlo simulation.

2 Theory

2.1 ϕ^4 Theory

ϕ^4 theory is described by the Lagrangian [1]

$$\mathcal{L} = \frac{1}{2}\left(\partial_\mu \phi\right)\left(\partial^\mu \phi\right) - \frac{1}{2}\mu^2\phi^2 - \frac{\lambda}{4!}\phi^4 \tag{1}$$

where $\phi = \phi(x)$ is a real scalar quantum field depending on the 4-vector x in Minkowski space-time, μ is the (bare) mass of the field and λ is its (bare) coupling constant.

Correlation functions are important quantities in any quantum field theory. In the path integral formalism the n-point correlation function C_n can be written as [2]:

$$C_n \coloneqq \langle\Omega|\, T\left(\phi(x_1)\dots\phi(x_n)\right)|\Omega\rangle = \lim_{t\to\infty(1-i\epsilon)} \frac{\int\mathcal{D}[\phi]\,\phi(x_1)\dots\phi(x_n)\exp\left(i\int_{-t}^{+t}\mathrm{d}^4x\mathcal{L}\right)}{\int\mathcal{D}[\phi]\,\exp\left(i\int_{-t}^{+t}\mathrm{d}^4x\mathcal{L}\right)} \tag{2}$$

where $|\Omega\rangle$ is the vacuum of the interacting field and T is the time ordering operator. The functional integral $\int\mathcal{D}[\phi]$ is understood to run over all possible fields $\phi(x)$. By rotating the time integration path slightly off the real axis into the complex plane, which is indicated by the ϵ term in the time limit, we introduce exponential damping to the fields, so that the path integral starts and ends with the vacuum state. Alternatively we can rotate the time integration path completely onto the imaginary axis by introducing imaginary time:

$$t = -i\tau \tag{3}$$

This called a Wick rotation. It allows us to write the derivatives in the Lagrangian (1) as

$$\left(\partial_\mu\phi\right)\left(\partial^\mu\phi\right) = \left(\partial_t\phi\right)^2 - \left(\nabla\phi\right)^2 = -\left(\left(\partial_\tau\phi\right)^2 + \left(\nabla\phi\right)^2\right) =: -\left(\partial^E\phi\right)^2 \tag{4}$$

which is just the Euklidean 4-dimensional derivative with an overall minus sign[1]. This places time and space on the same footage, which is advantageous for our implementation of a space-time lattice. We can rewrite equation 2 in Euklidean space-time [2]

$$C_n \coloneqq \langle\Omega|\, T\left(\phi(x_1^E)\dots\phi(x_n^E)\right)|\Omega\rangle = \frac{\int\mathcal{D}[\phi]\,\phi(x_1^E)\dots\phi(x_n^E)\exp\left(-S^E[\phi]\right)}{\int\mathcal{D}[\phi]\,\exp\left(-S^E[\phi]\right)} \tag{5}$$

[1] due to the particle physics convention for the Minkowski metric

with the Euklidean action $S^E[\phi]$, defined as

$$S^E[\phi] \coloneqq -iS[\phi] = -i \int \mathrm{d}^4x \mathcal{L} = \int \mathrm{d}^4x^E \left(\frac{1}{2} \left(\partial^E \phi \right)^2 + \frac{1}{2}\mu^2\phi^2 + \frac{\lambda}{4!}\phi^4 \right) \tag{6}$$

Note that the numerator in equation 5 plays the role of a partition function.

$$Z \coloneqq \int \mathcal{D}[\phi]\, e^{-S^E[\phi]} \tag{7}$$

From now on we will always work in Euklidean space-time unless explicitely stated. To ease notation we drop the superscript ^{E} in further equations.

2.2 The 2-point Correlator

We define the 2-point correlator $\tilde{C}_2(t)$ as the sum over all 2-point correlation functions, whose points differ only by a time t.

$$\tilde{C}_2(t) = \sum_{i=1}^{N} \langle \Omega |\, \phi(t, \vec{x}_i)\phi(0, \vec{x}_i)\, | \Omega \rangle \tag{8}$$

According to Montvay and Münster [3] this can be written as

$$\tilde{C}_2(t) = A \cdot e^{-m_{\mathrm{eff}}|t|} + \ldots \tag{9}$$

where the dots indicate terms, that fall off faster at large t. Here m_{eff} is the physical mass (as opposed to the bare mass μ) of the field and A is some constant factor. Thus for $t' > t \gg 1$:

$$\frac{\tilde{C}_2(t)}{\tilde{C}_2(t')} \approx e^{-m_{\mathrm{eff}}|t'-t|}$$

and

$$m_{\mathrm{eff}} \approx \log \left(\frac{\tilde{C}_2(t)}{\tilde{C}_2(t+1)} \right) \tag{10}$$

2.3 Spontaneous Symmetry Breaking

The potential part of the ϕ^4 Lagrangian (eq. 1) reads

$$V(\phi) = \frac{1}{2}\mu^2\phi^2 + \frac{\lambda}{4!}\phi^4$$

For $\lambda < 0$ the potential is not bound from below and hence there are no physical solutions. Therefore we will always assume $\lambda \geq 0$. For $\mu^2 > 0$ the potential has a minimum at $\phi = 0$ and is symmetric around this point. Thus the vacuum expectation value (vev) is $\langle \phi \rangle = 0$ and the symmetry of the theory is preserved. For $\mu^2 < 0$ the potential has two minima and looks like a sombrero, hence the name "mexican hat potential". The state $\phi = 0$ is unstable and spontaneous symmetry breaking occurs. The field "falls" into one of the two ground states, developing a vev $\langle \phi \rangle \neq 0$.

2.4 Effective Potential

After renormalization the effective potential of the theory is given by [4]

$$V_{\text{eff}}(\phi) = \frac{1}{2} m_{\text{eff}}^2 Z_\phi^{-1} \phi^2 + \frac{\lambda_{\text{r}}}{4!} Z_\phi^{-2} \phi^4 \tag{11}$$

where m_{eff} is the effective mass, λ_{r} is the renormalized coupling constant and Z_ϕ is the field strength renormalization constant. To determine the effective potential, we first introduce an auxiliary term to the potential, coupling the field to a constant external source J [4].

$$U(\phi) \coloneqq V_{\text{eff}}(\phi) - J\phi$$

The vacuum expectation value (vev) $\langle\phi\rangle$ in this potential depends on the current J. The exact dependence can be measured on the lattice. Inverting this relation, we can regard the current as a function of the vev $J = J(\langle\phi\rangle)$. The vev is the field at which the potential U is minimal. Therefore [4]

$$\frac{\partial U}{\partial \phi}\left(\langle\phi\rangle\right) = 0 = \frac{\partial V_{\text{eff}}}{\partial \phi}\left(\langle\phi\rangle\right) - J\left(\langle\phi\rangle\right)$$

The effective potential is therefore given by [4]

$$V_{\text{eff}} = \int_0^\phi \mathrm{d}\langle\phi\rangle J\left(\langle\phi\rangle\right) \tag{12}$$

3 Discretization

3.1 Classic Parametrization

We work on a d-dimensional lattice of length L_k in direction k, so that the lattice has a space-time volume of $V = \prod_{k=1}^d L_k$. The spacing between neighbouring sites is denoted by a_k, forming volume elements $v = \prod_{k=1}^d a_k$. Thus the lattice has $N = \prod_{k=1}^d L_k/a_k$ sites in total. At each lattice site x_i the field ϕ has a real value $\phi(x_i)$. As an approximation for the derivative of $\phi(x_i)$ in direction k we use

$$\partial_k \phi(x_i) = \frac{\phi(x_i + a_k \hat{e}_k) - \phi(x_i)}{a_k} \tag{13}$$

where $\hat{e}_k$ is a vector of unit length in direction k. To keep the derivatives well defined at the edges of the lattice, we use periodic boundary conditions. The discretized action is then given by:

$$S[\phi] = v \cdot \sum_{i=1}^N \left(\frac{\left(\phi(x_i + a_k\hat{e}_k) - \phi(x_i)\right)^2}{2a_k^2} + \frac{1}{2}\mu^2\phi(x_i)^2 + \frac{\lambda}{4!}\phi(x_i)^2 \right) \tag{14}$$

In the continuum limit ($a \to 0$ and $N \to \infty$ while keeping V constant) this is equivalent to the action given in equation 6. For our purposes the change in the action ΔS upon changing the field $\phi(x_j) \to \phi'(x_j)$ at a single site x_j is important.

$$\begin{aligned}
\Delta S \;=\; & \frac{v}{2} \sum_{k=1}^d \frac{\left[\phi(x_j + a_k\hat{e}_k) - \phi'(x_j)\right]^2 - \left[\phi(x_j + a_k\hat{e}_k) - \phi(x_j)\right]^2}{a_k^2} \\
& + \frac{v}{2} \sum_{k=1}^d \frac{\left[\phi(x_j - a_k\hat{e}_k) - \phi'(x_j)\right]^2 - \left[\phi(x_j - a_k\hat{e}_k) - \phi(x_j)\right]^2}{a_k^2} \\
& + \frac{v\mu^2}{2}\left(\phi'(x_j)^2 - \phi(x_j)^2\right) + \frac{v\lambda}{4!}\left(\phi'(x_j)^4 - \phi(x_j)^4\right)
\end{aligned} \tag{15}$$

In this parametization the lattice parameters μ^2 and λ are the same as the parameters of the ϕ^4 Lagrangian (eq. 1). This eases physical interpretation of certain effects. For example spontaneous symmetry breaking can be observed for $\mu^2 < 0$. Another advantage is, that it works for an arbitrary number d of space-time dimensions and non-isotropic lattices. For a 4-dimensional, isotropic lattice ($a_k = a \,\forall k \Rightarrow v = a^4$) equation 15 simplifies to

$$\begin{aligned} \Delta S &= -a^2 \left[\phi'(x_j)\phi(x_j)\right] \sum_{k=1}^{4} \left\{\left[\phi(x_j + a\hat{e}_k) + \phi(x_j - a\hat{e}_k)\right]\right\} \\ &\quad + \left(\frac{a^4\mu^2}{2} + 4a^2\right)\left(\phi'(x_j)^2 - \phi(x_j)^2\right) + \frac{a^4\lambda}{4!}\left(\phi'(x_j)^4 - \phi(x_j)^4\right) \end{aligned} \tag{16}$$

3.2 Alternative Parametrization

We are mainly interested to study ϕ^4 theory in 4 dimensions, i.e. 3 spatial and 1 time dimension in Euklidean space-time. To keep things simple and treat all dimensions equally, we choose to work on an isotropic lattice. In this case there is an interesting alternative parametrization [5].

By rescaling the field and introducing an alternative set of lattice parameters κ and α, which are defined by

$$\varphi = \frac{\sqrt{2}\kappa}{a}\phi \tag{17}$$

$$a^2\mu^2 = \frac{1 - 2\alpha}{\kappa} - 8 \tag{18}$$

$$\lambda = \frac{6\alpha}{\kappa} \tag{19}$$

we can rewrite equation 14 to

$$S[\varphi] = \sum_{i=1}^{N}\left(-2\kappa\sum_{k=1}^{4}\left[\varphi(x_i)\varphi(x_i + a\hat{e}_k)\right] + \varphi(x_i)^2 + \alpha\left[\varphi(x_i)^2 - 1\right]^2\right) \tag{20}$$

and accordingly

$$\begin{aligned} \Delta S &= -2\kappa\sum_{k=1}^{4}\left(\left[\varphi'(x_i) - \varphi(x_i)\right]\left[\varphi(x_i + a\hat{e}_k) + \varphi(x_i - a\hat{e}_k)\right]\right) \\ &\quad + \varphi'(x_i)^2 - \varphi(x_i)^2 + \alpha\left(\left[\varphi'(x_i)^2 - 1\right]^2 - \left[\varphi(x_i)^2 - 1\right]^2\right) \end{aligned} \tag{21}$$

This parametrization has the advantage, that all quantities are dimensionless. Additionally the coupling strength of neighbouring fields to each other is completely determined by κ. In analogy to solid-state theories, where such terms describe the probability of quanta to move ("hop") from one location of a crystal lattice to another, κ is called the hopping parameter [5].

3.3 Integration

The path integrals $\int \mathcal{D}[\phi]$ in equation 5 can be approximized by summing over a finite number of field configurations. However the integrand $e^{-S^E[\phi]}$ varies rapidly over many orders of magnitude and most field configurations contribute very little to the sum. To avoid wasting precious computing time on irrelevant field configurations, we perform "importance sampling".

Motivated by statistical mechanics, we sample field configurations $\phi_\nu(x)$ from a Boltzmann distribution [6]

$$P(\phi_\nu) = \frac{1}{Z} e^{-S[\phi_\nu]} = \frac{\exp\left(-S[\phi_\nu]\right)}{\int \mathcal{D}[\phi] \, \exp\left(-S[\phi]\right)} \tag{22}$$

An estimate for the n-point correlation function is then simply given by

$$\bar{C}_n = \frac{1}{M} \sum_{\nu=1}^{M} \left[\phi_\nu(x_1) \dots \phi_\nu(x_n)\right] \tag{23}$$

where M is the total number of sampled field configurations.

4 Algorithm

4.1 Metropolis-Hastings

Sampling from the Boltzmann distribution (eq. 22) is realized by a Markov chain Monte Carlo simulation using the Metropolis-Hastings algorithm. It works as follows:

1. Initialize the lattice with a constant initial field strength ϕ_{ini} at all sites.
2. Sweep over the lattice by performing the following steps at every lattice site x_j.
   a) Sample from a uniform distribution $\Delta\phi \in [-\delta_{\max}, \delta_{\max}]$ for some constant $\delta_{\max}$.
   b) Vary the field $\phi(x_j) \to \phi'(x_j) = \phi(x_j) + \Delta\phi$.
   c) Calculate the resulting change in the action ΔS (cf. eq. 15 & 21)
   d) Accept the variation of the field with a probability of $\rho = \min\left(1, e^{-\Delta S}\right)$, otherwise reject it.
3. Calculate an interesting quantity (e.g. the product of fields $[\phi_\nu(x_1) \dots \phi_\nu(x_n)]$) at the current state ν and store it.
4. Repeat the steps 2 and 3 M times.
5. Average over all stored values to get an estimate for the physical quantity (cf. eq. 23)

It is highly advisable to perform a number of sweeps before the first measurement (step 3), so that the lattice can "thermalize". This is especially important when the initial field strength ϕ_{ini} is very different from the fields expectation value $\langle\phi\rangle$. The time needed for thermalization also depends on the parameter $\delta_{\max}$. Small values of $\delta_{\max}$ lead to long thermalization times, because ϕ varies so little at every sweep. High values on the other hand also lead to long computation times, because in this case many proposed changes are rejected, so that ϕ does not change at all. From experience it seems to be advisable to choose $\delta_{\max}$ such that the acceptance is somewhere around 2/3.

To reduce correlation between subsequent measurements one can perform several sweeps between measurements (i.e. do step 2 w times before step 3). It should be noted that, given a suitable number of sweeps, the algorithm generates the correct distribution even when measurements are correlated, since detailed balance is still given. However correlation can produce difficulties during error estimation.

4.2 Bootstrap

Given a sample $\{\beta[\phi]\}$ of some observable β, generated by a Markov chain, the mean of that sample is a good estimate $\bar{\beta}$ for the observable. The bootstrap algorithm is a method to acquire an estimate for the error aswell. It generates new samples $\left\{\beta^b[\phi]\right\}$ by randomly sampling elements of the original sample. That way R bootstrap samples of the same length as the original sample are generated. Then for each sample a bootstrap estimate $\bar{\beta}^b$ for the observable is calculated by taking the mean of each bootstrap sample. The estimate for the error is the standard deviation of the bootstrap estimates [7].

$$\delta\beta^{bs} = \mathrm{std}\left(\bar{\beta}^b\right) \tag{24}$$

5 Measurement and Analysis

We implement the lattice, the Metropolis-Hastings algorithm and the bootstrap algorithm in `python`. For simplicity we choose to always use unit spacings $a = 1$ and work in an isotropic lattice with n sites in each direction. In sections 5.2, 5.3 and 5.5 we work with both parametrizations, the subsequent sections we stick to the classic parametrization. In sections 5.1 we test our algorithm in 1 and 2 dimensions respectively, in all other sections we work in $d = 4$ dimensions.

5.1 Testing the Code

To verify that our algorithm works correctly we replicate figure 5 from a paper of Creutz and Freedman [6]. We run the program with $d = 1$, $\mu^2 = 1$, $\lambda = 0$, $n = 1000$, $M_{\text{therm}} = 50$, $M = 1000$ and $w = 4$. We create a histogram of all field values at all lattice sites and compare it to the theoretical solution for the continuum

$$|\Psi|^2(\phi) = \sqrt{1/\pi} \cdot \exp(-\phi^2)$$

and the lattice solution

$$|\Psi|^2(\phi) = \sqrt{\omega/\pi} \cdot \exp(-\omega\phi^2) \quad \text{with} \quad \omega = \sqrt{\mu^2(1+a^2)\mu^2/4}$$

which are both given in [6]. Our results are shown in figure 1.

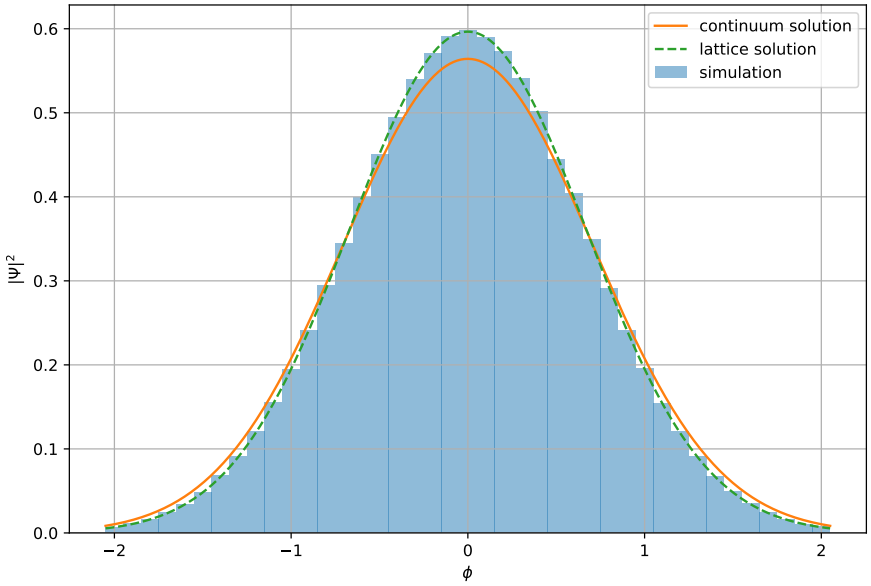

Figure 1: Plot of $|\Psi|^2$ in dependence of ϕ

The simulation matches the expected lattice solution almost perfectly. We conclude that it works as intended.

To perform a first exploration of the effect of spontaneous symmetry breaking we simulate a lattice with $d = 2$, $M_{\text{therm}} = 50$, $w = 4$, $n = 30$, $\mu^2 = -1$ and $\lambda = 1$. The result is shown in figure 2.

One can clearly see the effect of the symmetry breaking as parts of the field fall into the wells of the "mexican hat potential".

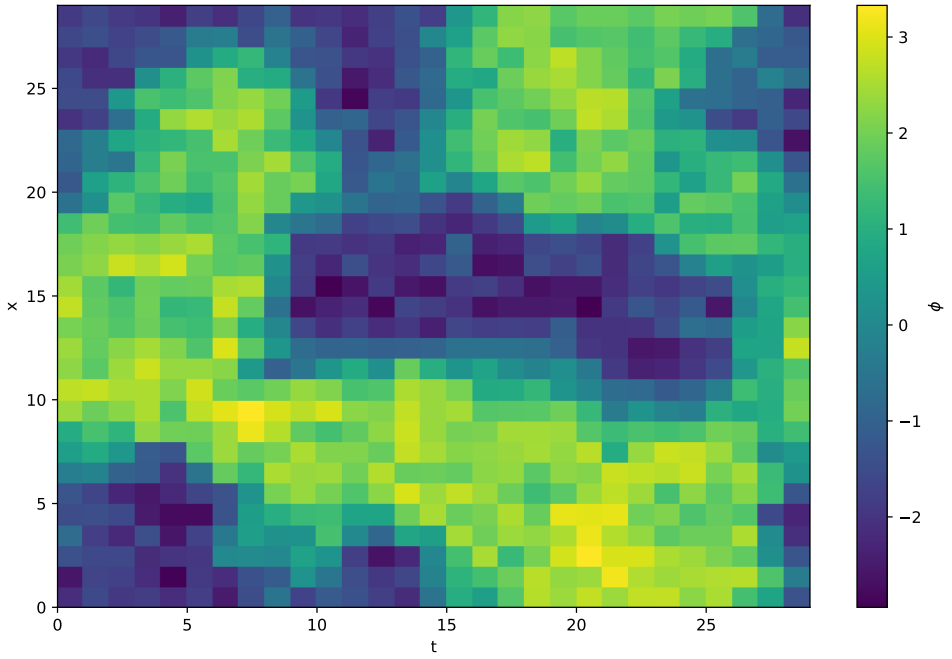

Figure 2: Plot of ϕ in dependence of t and x

5.2 Acceptance Optimization

To achieve an acceptance between 60 % and 70 % we calculate $\delta_{\max} = \sqrt{a \cdot G}$ [6] with a variable parameter G. This allows $\delta_{\max}$ to grow with the lattice spacing, should we choose to change it. We vary the free parameter G with the settings $N = 10$, $M = 50$, $w = 4$ and $\phi_{\text{ini}} = 0.1$. For the classic parametrization we use $\mu^2 = \lambda = 1$, for the alternative one we use $\kappa = \alpha = 1$. The resulting acceptance measurements are shown in figure 3.

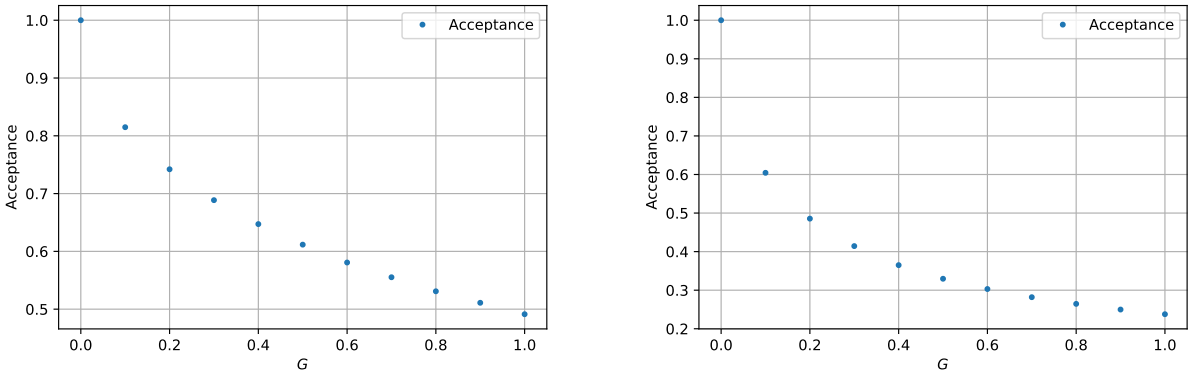

(a) Classic parametrization

(b) Alternative parametrization

Figure 3: Plot of the acceptance in dependence of G with $\delta_{\max} = \sqrt{a \cdot G}$

We choose $G = 0.3$ for the classic and $G = 0.08$ for the alternative parametrization for all further measurements.

We also use the runtime of this analysis as an indicator for the speed of our simulation. On our machine the algorithm based on the classic parametrization completes one set of sweeps in 266(2) s, the algorithm based on the alternative parametrization in 120(1) s. This is in

agreement with our expectation since the alternative parametrization is limited to equal lattice spacing and $d = 4$. These limitations are used to simplify the calculations and therefore the algorigthm runs faster.

5.3 Thermalization Analysis

To determine the optimal amount of thermalization steps we use the vacuum expectation value $\langle\phi\rangle$ of the field as an indicator. For the classic parametrization we vary μ^2 and λ and for the alternative parametrization we vary κ and α. In addition we vary $\phi_{\text{ini}} = 0.1$ for both and we try to cover the values used in our further analysis. We use $n = 10$ as we are going to do for the further analysis. The parameter w is set to 1 so that we can observe changes after each sweep. Figures 4 and 5 show the resulting plots.

In the classic parametrization the system diverges for $\lambda < 0$ and $\mu^2 < 0$, $\lambda = 0$ since the potential becomes unbound from below. When $\mu^2 > 0$ and $\lambda > 0$ the system converges to $|\langle\phi\rangle| = 0$ within 100 sweeps even for high ϕ_{ini}. For such an unbroken symmetry neither μ^2 nor λ have an effect on the value of $|\langle\phi\rangle|$, however a higher value of λ seems to speed up the process. For a broken symmetry with $\mu^2 < 0$ and $\lambda > 0$ a higher μ^2 aswell as a lower λ corresponds to deeper and wider "mexican hat potential", moving the minima outwards, so that the system converges to a higher value. In the broken symmetry case the choice of $\phi_{\text{ini}} > 0$ significantly reduces the convergence time from over 250 sweeps to under 200.

In the alternative parametrization the system diverges when $\alpha \leq 0$. This is clear from equations 18 and 19. A larger value of α decreases the value the system converges towards. For small values of α the convergence time stays roughly constant, but increases for larger ones. When $\kappa \leq 0$ the system converges quickly to $|\langle\varphi\rangle| = 0$ since the fields are either not coupled or anti-coupled and therefore average out to 0. For larger values of κ the value, to which the system converges, increases and the convergence time increases roughly proportionally. Any value of φ_{ini} that is larger than zero leads to a dramatic decrease in convergence time. $|\langle\varphi\rangle|$ generally converges within 50 sweeps when φ_{ini} is set to 0.1.

Based on these observations we choose $\phi_{\text{ini}} = 0.1$ and $M_{\text{therm}} \cdot w = 200$ for the classic parametrization and $\varphi_{\text{ini}} = 0.1$ and $M_{\text{therm}} \cdot w = 100$ since $|\langle\phi\rangle|$ and $|\langle\varphi\rangle|$ converge within these parameters for all tested setups. All measurements in the following sections will be done with these thermalization settings.

5.4 Finite Size Analysis

The lattice shape n that we use has an effect on both the runtime of our code as well as on the accuracy of the measured values. Since we only have a limited amount of time available and do not need exceeding amounts of accuracy we want to select a value that provides a balance of both. To make this selection we vary n and determine the effective mass m_{eff} with $\mu^2 = \lambda = 1$ for the classic parametrization and $\kappa = \alpha = 1$ for the alternative parametrization. The results are shown in figure 6.

Both the error and value converge quickly towards the average when using the classic parametrization. This convergence of the error is expected since the number of lattice sites growths like $N = n^d$. Every added lattice site increases the amount of data points used for our measurements, therefore the error reduces roughly $\propto n^{-d/2}$. The alternative parametrization cannot be used due to an error in section 5.5.

We choose $n = 10$ for our further analysis since the relative accuracy of 0.7 % for the classic parametrization is sufficient for our needs while the runtimes remain reasonable.

5.5 Correlator Extraction

We use the settings $\mu^2 = \lambda = 1$ for the classic parametrization and $\kappa = \alpha = 1$ for the alternative one. We extract the 2-point-correlator $\tilde{C}_2(t)$ by calculating $\sum_x \phi(t,x)\phi(0,x)$ in every measurement step. Since we use periodic boundary conditions we can only calculate this for $t \leq \lfloor n/2 \rfloor = 5$, but we can use all lattice sites for the calculation. With this we average the correlators over the entire temporal axis of the lattice and the entire Markov Chain. Then we normalize them by dividing them by $\tilde{C}_2(0)$. Figure 7 shows an example of this.

We perform a fit of the function $\tilde{C}_2(t)/\tilde{C}_2(0) = \exp(P \cdot t)$ to the data points of the classic parametrization. The resulting χ^2/n.d.f. is 1.61, suggesting a very good match of the function to the data points, in good agreement with our theory. The parameter P was determined to be 1.962(11).

For the alternative parametrization this procedure fails for some yet unknown reason. Therefore we will only use the classic parametrization for further analysis.

5.6 Effective Mass Measurements

We want to determine the value of μ^2 at which the spontaneous symmetry breaking occurs in dependence of λ.

For the classic parametrization we create a lattice and measure m_{eff} for different values of λ and varying μ^2. The results are shown in figure 8.

For all values of λ we can observe a breakdown of the calculation method for m_{eff} for different negative values of μ^2. To determine the critical point at which this breakdown occurs we fit the following function to the data:

$$m_{\text{eff}}(\mu^2) = \begin{cases} 1 + \operatorname{erf}\left(P_3(P_0 - P_4)\right) \cdot P_5/2 + P_2(\mu^2 - P_0) & \text{if } \mu^2 \geq P_0 \\ 1 + \operatorname{erf}\left(P_3(\mu^2 - P_4)\right) \cdot P_5/2 & \text{if } \mu^2 < P_0 \end{cases}$$

These fits only match the data points to a very limited degree, which is evident from their very high χ^2/n.d.f. of more than 180. Clearly this function is not well suited to describe the physics of the effect. However the parameter P_0 is an acceptable rough estimate for the point at which the breakdown occurs. The values of this parameter can be found in table 1.

λ	20	30	40	50
P_0	-0.12	-0.73	-1.29	-2.01

Table 1: Fit parameter P_0 for figure 8

We do not list the errors of these parameters since they are of the order of 10^2. This is another result of the bad fit.

5.7 Effective Potential

Finally we want to determine the effective potential. Following section 2.4 we introduce the term $J\phi$ to the potential. Then we measure the vacuum expectation values $\langle\phi\rangle$ for varying currents J and fit the following function to the data [4]:

$$J(\phi) = a\phi + \frac{b}{6}\phi^3$$

This procedure is done once with a broken symmetry with parameters $\mu^2 = -1$ and $\lambda = 2$ and once with an unbroken symmetry with parameters $\mu^2 = \lambda = 1$. To observe the effective potential V_{eff} we integrate $J(\phi)$ 12. The fits are shown in figures 9 and 10.

Additionally the effective mass m_{eff} is extracted by the same method as described in section 5.6. Then we determine the renormalized coupling constant λ_{r} and the field strength renormalization constant Z_ϕ by [4]

$$Z_\phi \quad = \quad \frac{m_{\text{eff}}^2}{a}\lambda_{\text{r}} = bZ_\phi^2$$

The resulting values are shown in table 2.

	m_{eff}	Z_ϕ	λ_{r}
Broken	0.040(13)	−0.0018(11)	6.4(83)
Unbroken	1.968(11)	3.657(42)	13.21(31)

Table 2: Fit parameter P_0 for figure 8

The values for the broken case suffer from the inaccurate determination of m_{eff} due to the breakdown of our method.

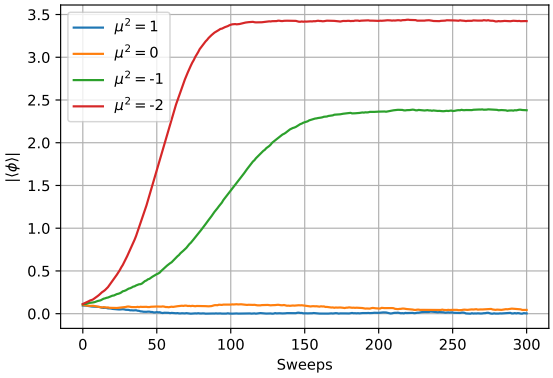

(a) Varying μ^2 with $\lambda = 1$ and $\phi_{\text{ini}} = 0.1$

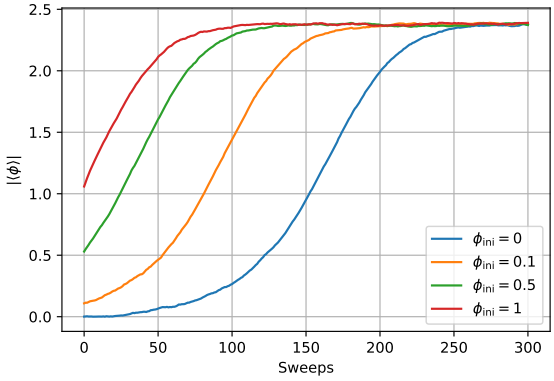

(b) Varying ϕ_{ini} with $\mu^2 = -1$ and $\lambda = 1$

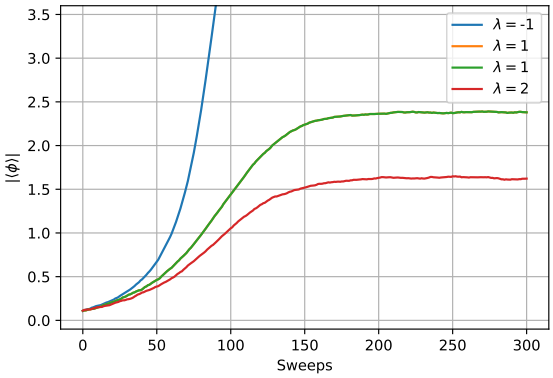

(c) Varying λ with $\mu^2 = -1$ and $\phi_{\text{ini}} = 0.1$

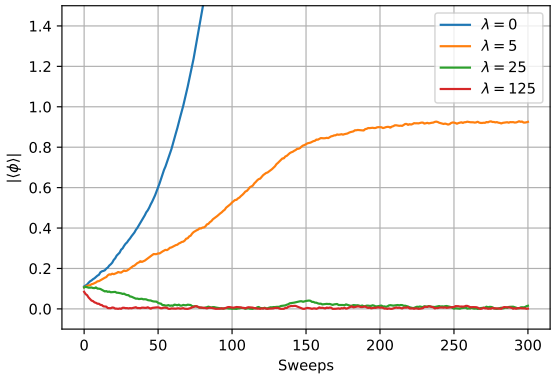

(d) Varying λ with $\mu^2 = -1$ and $\phi_{\text{ini}} = 0.1$

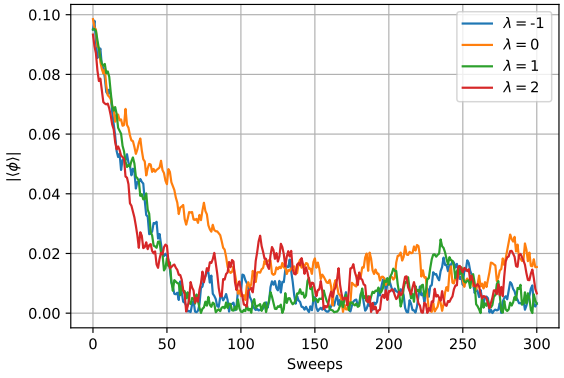

(e) Varying λ with $\mu^2 = 1$ and $\phi_{\text{ini}} = 0.1$

Figure 4: Plots of $|\langle\phi\rangle|$ in dependence of the amount of sweeps and varying parameters for the classic parametrization

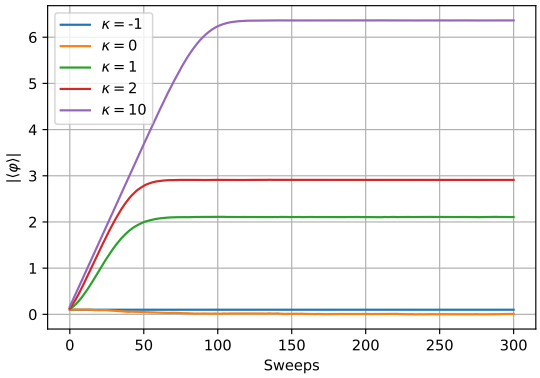

(a) Varying κ with $\alpha = 1$ and $\varphi_{\text{ini}} = 0.1$

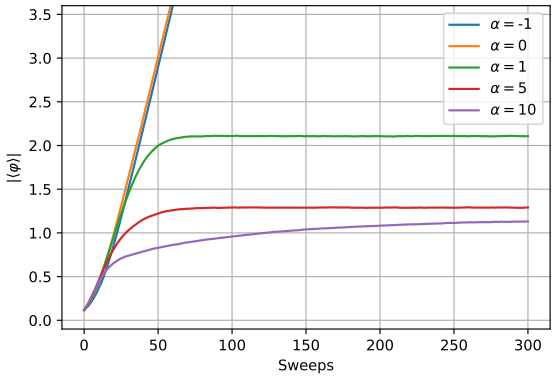

(b) Varying α with $\kappa = 1$ and $\varphi_{\text{ini}} = 0.1$

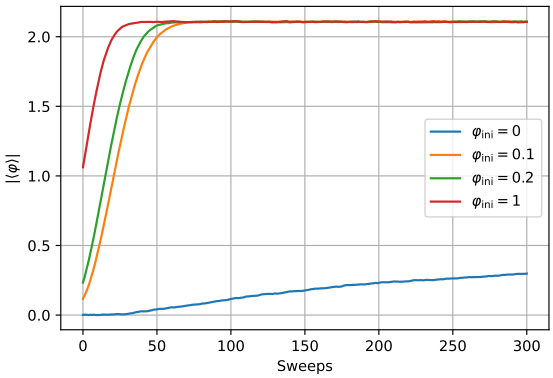

(c) Varying φ_{ini} with $\kappa = \alpha = 1$

Figure 5: Plots of $|\langle\varphi\rangle|$ in dependence of the amount of sweeps and varying parameters for the alternative parametrization

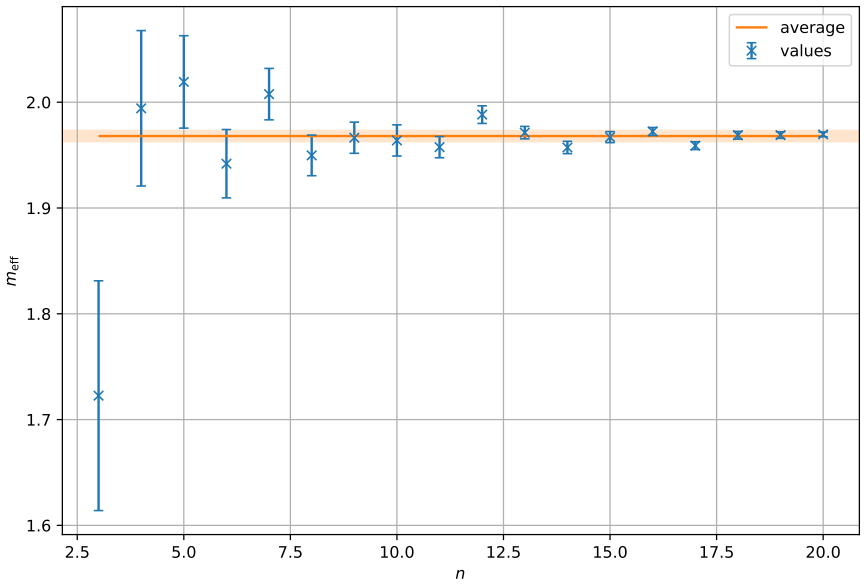

Figure 6: Plot of m_{eff} in dependence of N with $\mu^2 = \lambda = a = 1$

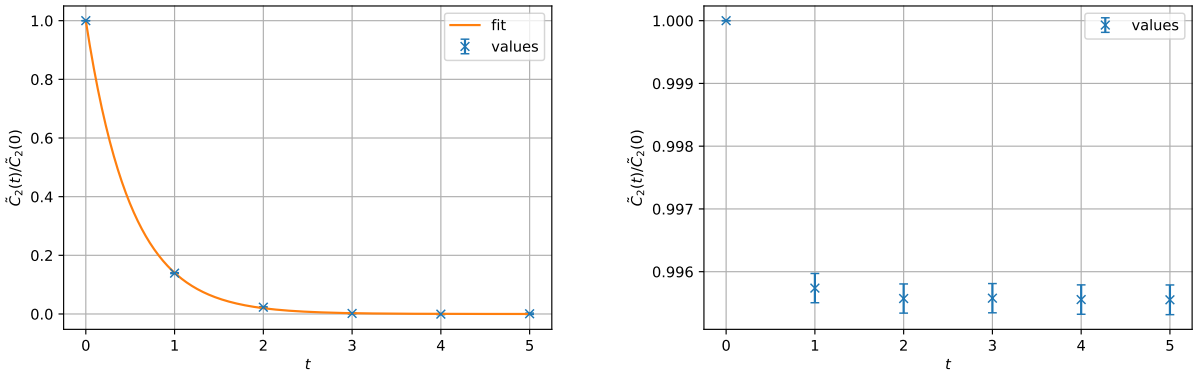

(a) Classic parametrization (b) Alternative parametrization

Figure 7: Normalized 2-point correlators

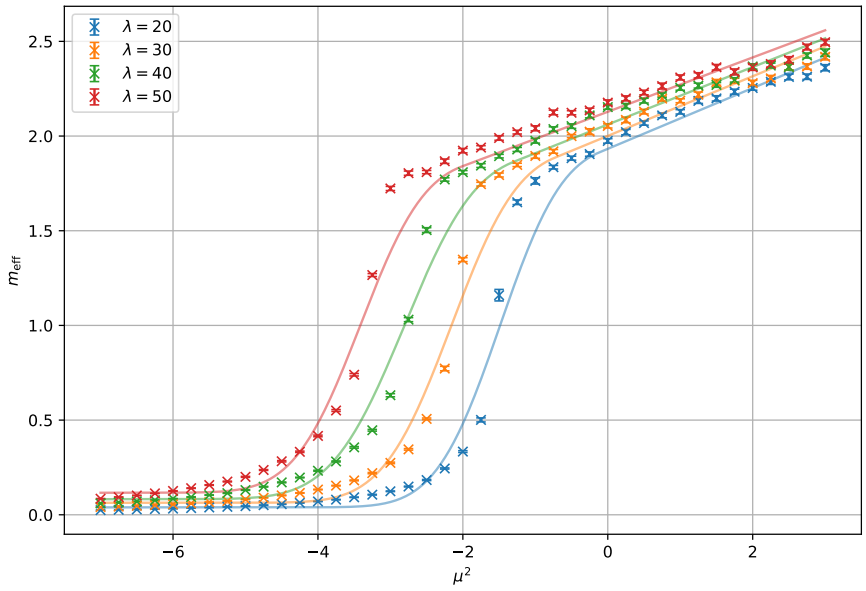

Figure 8: Plot of m_{eff} in dependence of μ^2 for varying λ

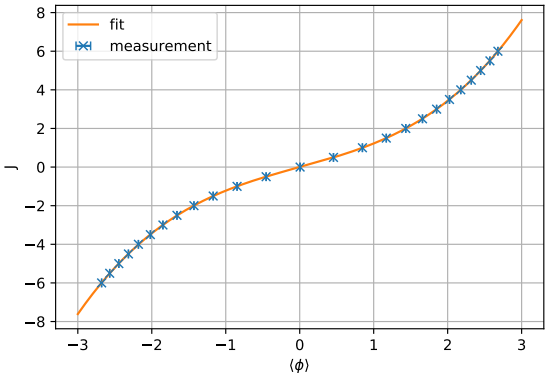

(a) $J(\langle\phi\rangle)$

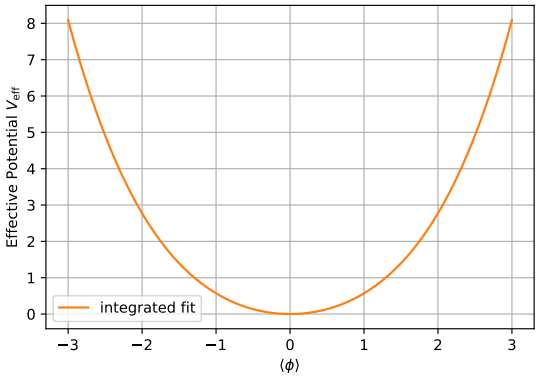

(b) Effective potential V_{eff}

Figure 9: Measurements for the effective potential with $\mu^2 = \lambda = 1$

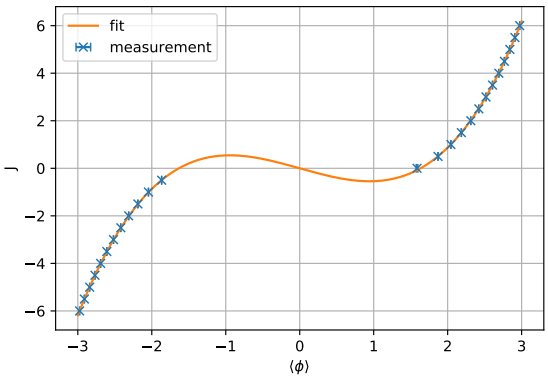

(a) $J(\langle\phi\rangle)$

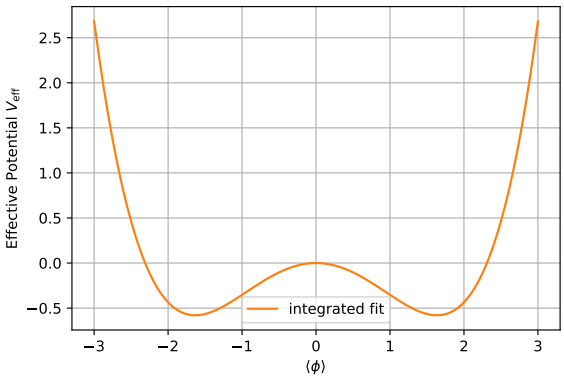

(b) Effective potential V_{eff}

Figure 10: Measurements for the effective potential with $\mu^2 = -1$ and $\lambda = 2$

6 Summary

We successfully implement a Markov chain Monte Carlo simulation for phi^4 theory based on the Metropolis-Hastings algorithm. The classic parametrization of the change in action seems to work just fine, while our implementation of the alternative parametrization, although certainly interesting, seems to be faulty. We successfully recreated a result from Creutz and Freedmans paper and depicted spontaneous symmetry breaking. We successfully optimized the acceptance of our code, chose an appropriate thermalization procedure and lattice size and extracted 2-point correlators and effective masses. Using the classic parametrization we managed to extract the full effective potential.

References

[1] Michael E Peskin and Daniel V Schroeder. *An introduction to quantum field theory*. Westview, Boulder, CO, 1995. Includes exercises.

[2] Hans Jockers. Lecture notes on advanced quantum field theory, 2020. University of Bonn.

[3] Istvan Montvay and Gernot Münster. *Quantum Fields on a Lattice*. Cambridge Monographs on Mathematical Physics. Cambridge University Press, 1994.

[4] M Jansen and K Nickel. ϕ^4 theory on the lattice. *HISKP*, March 2011.

[5] Axel Maas. Lecture notes on lattice quantum field theory, 2017. KFU Graz.

[6] M Creutz and B Freedman. A statistical approach to quantum mechanics. *Annals of Physics*, 132(2):427–462, 1981.

[7] Thomas Luu. Lecture on computational physics, 2020. University of Bonn.